

# THE KERNEL METHOD FOR ELECTRICAL RESISTANCE TOMOGRAPHY

ANTONELLO TAMBURRINO<sup>1</sup>, VINCENZO MOTTOLA<sup>1</sup>

**Abstract.** This paper treats the inverse problem of retrieving the electrical conductivity starting from boundary measurements in the framework of Electrical Resistance Tomography (ERT). In particular, the focus is on non-iterative reconstruction methods that are compatible with real-time applications.

In this work, the Kernel Method, a new non-iterative reconstruction method for Electrical Resistance Tomography, is presented. The imaging algorithm deals with the problem of retrieving one or more anomalies of arbitrary shape, topology, and size, embedded in a known background (inverse obstacles problem).

The foundation of the Kernel Method is that if there exists a proper current density applied at the boundary (Neumann data) of the domain that is able to produce the same measurements with and without the anomaly, then this boundary source produces a power density that vanishes in the region occupied by the anomaly, when applied to the problem involving the background material only.

Therefore, the Kernel Method consists of (i) evaluating a proper current density  $g$  at the boundary of the domain of interest, by solving a proper linear eigenvalue problem, (ii) solving one direct problem for the configuration without anomaly and driven by  $g$ , and (iii) reconstructing the anomaly as the region in which the power density is negligible.

This new tomographic method has a very simple numerical implementation that requires a very low computational cost.

In addition to theoretical results, an extensive numerical campaign proves the effectiveness of this new imaging method.

**Keywords:** Inverse electrical conductivity problem, Kernel Method, shape reconstruction, Electrical Resistance Tomography.

**MSC 2010:** 35R30, 35Q60, 35J25.

## 1. INTRODUCTION

Electrical Resistance Tomography (ERT) is a widely used tomographic inspection method that aims to retrieve the electrical conductivity  $\sigma$  inside a physical body, starting from boundary measurements of currents and voltages, in steady-state operation. Throughout the years, it has been successfully applied to a wide

---

<sup>1</sup>Dipartimento di Ingegneria Elettrica e dell'Informazione "M. Scarano", Università degli Studi di Cassino e del Lazio Meridionale, Via G. Di Biasio n. 43, 03043 Cassino (FR), Italy.  
Email: antonello.tamburrino@unicas.it (*corresponding author*), vincenzo.mottola@unicas.it.

range of different applications such as the petroleum and chemical process industry [1, 2, 3], medicine [4] (for cranial imaging [5], lung monitoring [6, 7], thermal monitoring of hyperthermia treatment [8], pediatric lung disease [9], breast imaging [10] and brain imaging [11]), semiconductor manufacturing [12], civil engineering [13], carbon nanotube manufacturing [14], biological culture analysis [15] and so on.

Different approaches to solving the ERT problem can be found in the literature, leading to two main classes: iterative and non-iterative imaging methods. The majority of the reconstruction methods are based on the iterative minimization of a proper cost function encoding the “distance” between the measured and synthetic data for the current estimate of  $\sigma$ , and proper a priori information. A list of references to this kind of approach can be found in [16]. These methods can achieve a good overall quality for the reconstructions. Still, they are (i) affected by the local minima problem, i.e. they are prone to false solutions, and (ii) computationally expensive because of the ill-posedness and the nonlinearity of the underlying inverse problem that calls for a large number of iterations.

The other class is that of non-iterative methods, where a proper indicator function is identified and utilized to provide reconstructions in just one step. The main advantage of this approach is the ability to achieve real-time performances, which is a feature as rare as it is required in applications. There are few non-iterative methods available in literature. The first one to be proposed is the Linear Sampling Method by Colton and Kirsch [17], followed by the Factorization Method by Kirsch [18, 19] and the Enclosure Method [20] proposed by Ikehata. A method based on the MUSIC signal processing algorithm has been also introduced by Devaney in [21], while the Monotonicity Principle Method was proposed by Tamburrino and Rubinacci in 2002 [22, 23].

This paper contributes to enlarging the class of non-iterative methods for ERT. Specifically, a new real-time inversion method is proposed for the inverse obstacle problem, where the aim is to retrieve the shape, position, and dimension of one or more anomalies of arbitrary size and topology embedded in a known background.

The method is based on some peculiar properties of the Neumann-to-Dirichlet operator, i.e. the operator  $\Lambda : g \mapsto u|_{\partial\Omega}$  mapping the electrical current injected into the domain  $\Omega$  through its boundary  $\partial\Omega$  and the corresponding scalar potential  $u$  evaluated on  $\partial\Omega$ .

Specifically, this paper proves that when a boundary data  $g$  makes the difference  $(\Lambda_{\sigma_D} - \Lambda_{bg})g$  negligible, then the ohmic power density  $p_{BG}(x)$  is almost vanishing in the region  $D$  occupied by the defect(s). Here,  $p_{BG}(x)$  refers to the power density in  $\Omega$  for the reference configuration where the anomaly is absent, while  $\Lambda_D$  and  $\Lambda_{bg}$  are the Neumann-to-Dirichlet operators in the presence of the anomaly  $D$  and for the reference configuration, respectively.

The real-time inversion method is then easily derived as (i) evaluate the aforementioned boundary data  $g$  starting from the measurement of  $\Lambda_D$ , (ii) compute

$p_{BG}(x)$ , the ohmic power density in  $\Omega$  for the reference configuration when  $g$  is applied to the boundary  $\partial\Omega$ , and (iii) reconstruct the anomaly as the region in which  $p_{BG}(x)$  is almost vanishing.

The paper is organized as follows. In Section 2 the problem is stated and some important properties of NtD map are recalled; in Section 3 the main idea behind the method is presented, together with the role of the Unique Continuation Principle; in Section 4 the main result is stated and a first reconstruction algorithm is given; in Section 6 the method is applied to first cases of study, where the NtD operator can be analytically evaluate and the data are noise-free; in Section 5 the treatment of the noise is proposed, together with the final version of the reconstruction algorithm. The numerical results are in Section 7, while the conclusions are drawn in Section 8.

## 2. STATEMENT OF THE PROBLEM

Throughout this paper,  $\Omega \subset \mathbb{R}^n$ , with  $n \geq 2$ , is the region occupied by the conducting material. It is assumed  $\Omega$  to be a simply connected and bounded domain with smooth boundary. The normal derivative defined on  $\partial\Omega$  is denoted as  $\partial_n$ .

Hereafter, for the convenience of the reader, the definition of the functional spaces underlying the mathematical formulation of the problem are recalled

$$\begin{aligned} H_\diamond^1(\Omega) &= \{u \in H^1(\Omega) \mid \int_{\partial\Omega} u(x) dx = 0\} \\ H_\diamond^{\pm 1/2}(\partial\Omega) &= \{u \in H^{\pm 1/2}(\partial\Omega) \mid \int_{\partial\Omega} u(x) dx = 0\} \\ L_\diamond^2(\partial\Omega) &= \{u \in L^2(\partial\Omega) \mid \int_{\partial\Omega} u(x) dx = 0\} \\ L_+^\infty(\Omega) &= \{u \in L^\infty(\Omega) \mid \text{ess sup}_{x \in \Omega} u(x) > 0\}. \end{aligned}$$

Assuming a linear and isotropic conductive material in  $\Omega$ , the constitutive relationship relating the electrical current density  $\mathbf{J}$  to the electric field  $\mathbf{E}$  is  $\mathbf{J}(x) = \sigma(x)\mathbf{E}(x)$ , where  $\sigma \in L_+^\infty(\Omega)$  is the electrical conductivity.

In terms of the electric scalar potential  $u$ , the steady current problem is formulated as

$$\begin{cases} \nabla \cdot (\sigma(x)\nabla u(x)) = 0 & \text{in } \Omega, \\ \sigma(x)\partial_n u(x) = g(x) & \text{on } \partial\Omega, \end{cases} \quad (2.1)$$

where  $u \in H_\diamond^1(\Omega)$ ,  $g \in H_\diamond^{-1/2}(\partial\Omega)$  is the prescribed normal component of the current density entering the domain  $\Omega$ , and  $\mathbf{E}(x) = -\nabla u(x)$ .

Problem (2.1) is meant in weak form, that is

$$\int_\Omega \sigma(x)\nabla u(x) \cdot \nabla \varphi(x) dx = \int_{\partial\Omega} g(x)\varphi(x) dx \quad \forall \varphi \in H_\diamond^1(\Omega). \quad (2.2)$$

The Neumann-to-Dirichlet (NtD) operator, which plays a key role since it represents the boundary measurements, maps the current flux  $g$  applied to the boundary

$\partial\Omega$ , to the corresponding electric scalar potential evaluated on  $\partial\Omega$ , i.e.  $u|_{\partial\Omega}$

$$\Lambda_\sigma : g \in H_\diamond^{-1/2}(\partial\Omega) \rightarrow u|_{\partial\Omega} \in H_\diamond^{1/2}(\partial\Omega).$$

The NtD operator has the following key properties.

**Property 1** (see [19, 24]).  $\Lambda_\sigma : L_\diamond^2(\partial\Omega) \rightarrow L_\diamond^2(\partial\Omega)$  is compact, self-adjoint and positive .

**Property 2** (see [24]).  $\Lambda_\sigma$  is monotonically decreasing in  $\sigma$ , i.e.,

$$\langle g, \Lambda_{\sigma_2}(g) \rangle \geq \langle g, \Lambda_{\sigma_1}(g) \rangle \quad \text{for } \sigma_2 \leq \sigma_1,$$

where  $\sigma_2 \leq \sigma_1$  means that  $\sigma_2(x) \leq \sigma_1(x)$  a.e. in  $\Omega$ .

**Lemma 2.1** (see [25, 26, 27]). Let  $\sigma_1, \sigma_2 \in L_+^\infty(\Omega)$  be two electrical conductivities and let  $u_i \in H^1(\Omega)$  be the solution of the Neumann problem

$$\nabla \cdot (\sigma_i(x) \nabla u_i(x)) = 0 \text{ in } \Omega \quad \text{and} \quad \sigma_i(x) \partial_n u_i(x) = g(x) \text{ on } \partial\Omega,$$

then

$$\int_\Omega (\sigma_2 - \sigma_1) |\nabla u_2|^2 dx \leq \langle (\Lambda_{\sigma_1} - \Lambda_{\sigma_2})(g), g \rangle \leq \int_\Omega \frac{\sigma_2}{\sigma_1} (\sigma_2 - \sigma_1) |\nabla u_2|^2 dx$$

The inverse problem in Electrical Resistance Tomography, as stated by Calderón [28], is to reconstruct the electric conductivity  $\sigma$  from the knowledge of  $\Lambda_\sigma$ . Given this framework, the present contribution is focused on the problem of retrieving the shape of one or more anomalies  $D_1, D_2, \dots$ , embedded in a known background. In other words, let  $D = \bigcup_j D_j$ , we consider an electrical conductivity  $\sigma_D$  of the form

$$\sigma_D(x) = \begin{cases} \sigma_{bg}(x) & x \in \Omega \setminus D, \\ \sigma_a(x) & x \in D, \end{cases} \quad (2.3)$$

where  $\sigma_{bg}$  is known, whereas domains  $D_1, D_2, \dots$  are unknown.

We define

$$\sigma_{bg}^m = \text{ess inf}_{x \in \Omega} \sigma_{bg}(x), \quad \sigma_{bg}^M = \text{ess sup}_{x \in \Omega} \sigma_{bg}(x)$$

and

$$\sigma_a^m = \text{ess inf}_{x \in \Omega} \sigma_a(x), \quad \sigma_a^M = \text{ess sup}_{x \in \Omega} \sigma_a(x).$$

and we require that  $\sigma_a$  and  $\sigma_{bg}$  are well-separated, in the sense that

$$\sigma_a^M(x) < \sigma_{bg}^m \quad \text{or} \quad \sigma_a^m(x) > \sigma_{bg}^M(x).$$

The target is to reconstruct the shape  $D$  of the region occupied by the anomalies. Each  $D_i$  is assumed connected and the  $D_i$ s are assumed disjoint.

Through the paper we denote with  $u_D$  the solution of problem (2.1) when the electric conductivity is  $\sigma_D$  and with  $u_{bg}$  the solution of the same problem when the electric conductivity is equal to  $\sigma_{bg}$  on the whole domain. Furthermore  $\Lambda_D$  and  $\Lambda_{bg}$  are the NtD operators related to the electrical conductivities  $\sigma_D$  and  $\sigma_{bg}$ , respectively.

## 3. UCP AND KERNEL METHOD

The starting point for the proposed method, hereafter named as Kernel Method (KM), is inspired by physical arguments.

Let us consider two different configurations: the actual one in the presence of the anomalies, described by the electrical conductivity  $\sigma_D$ , and a second configuration with the background electrical conductivity  $\sigma_{bg}$  in the whole domain ( $D = \emptyset$ ). The second configuration is termed as the *reference configuration*.

The Kernel Method is based on the following ideas. First, if, for a proper boundary data  $g$  the electrical current density, in both the actual and the reference configuration, does not flow through the anomalous region  $D$ , then the voltage measurements on the boundary are the same, i.e.  $\Lambda_D g = \Lambda_{bg} g$ . Second, if there exists a boundary data  $g$  giving the same boundary scalar potential with and without the anomaly, i.e. such that  $\Lambda_D g = \Lambda_{bg} g$ , then the corresponding electric current density for the reference configuration vanishes in  $D$ , as proved in the following results.

**Lemma 3.1.** *Let  $\sigma_D$  be the electrical conductivity defined in (2.3) and  $\sigma_{bg}$  be the known background conductivity. Then*

$$\langle (\Lambda_D - \Lambda_{bg}) g, g \rangle = 0 \iff \int_D \sigma_{bg}(x) |\nabla u_{bg}(x)|^2 dx = 0, \quad (3.1)$$

where  $u_{bg}$  is the solution of

$$\nabla \cdot (\sigma_{bg} \nabla u_{bg}(x)) = 0 \text{ in } \Omega \quad \text{and} \quad \sigma_{bg}(x) \partial_n u_{bg}(x) = g(x) \text{ on } \partial\Omega.$$

*Proof.* Without loss of generality, only the case  $\sigma_a^M < \sigma_{bg}^m$  is considered. The other case can be treated with similar arguments.

Applying Lemma 2.1 in the setting  $\sigma_1 = \sigma_D$  and  $\sigma_2 = \sigma_{bg}$ , and with some straightforward manipulations, it follows

$$k_l \int_D \sigma_{bg} |\nabla u_{bg}|^2 dx \leq \langle (\Lambda_D - \Lambda_{bg}) g, g \rangle \leq k_u \int_D \sigma_{bg} |\nabla u_{bg}|^2 dx. \quad (3.2)$$

with  $k_l$  and  $k_u$  two constants independent from the applied boundary data  $g$  and the shape or position of the anomaly  $D$ , specifically

$$k_l = \frac{\sigma_{bg}^m - \sigma_a^M}{\sigma_{bg}^M}, \quad k_u = \frac{\sigma_{bg}^M - \sigma_a^m}{\sigma_a^m}.$$

Since both  $k_l$  and  $k_u$  are positive because of the assumption  $\sigma_a^M < \sigma_{bg}^m$ , equation (3.2) implies that

$$\langle (\Lambda_D - \Lambda_{bg}) g, g \rangle = 0 \iff \int_D \sigma_{bg} |\nabla u_{bg}|^2 dx = 0.$$

□

**Corollary 3.2.** *Let  $\sigma_D$  be the electrical conductivity defined in (2.3) and  $\sigma_{bg}$  be the known background conductivity. Then*

$$\Lambda_D g = \Lambda_{bg} g = 0 \iff \int_D \sigma_{bg}(x) |\nabla u_{bg}(x)|^2 dx = 0,$$

where  $u_{bg}$  is as in Lemma 3.1.

*Proof.* Assuming  $\sigma_D < \sigma_{bg}$ , the Monotonicity Principle (see Property 2) gives  $\Lambda_D - \Lambda_{bg} \geq 0$ . Then, from standard linear algebra arguments, it results

$$\Lambda_D g = \Lambda_{bg} g \iff \langle (\Lambda_D - \Lambda_{bg}) g, g \rangle = 0, \quad (3.3)$$

and, therefore, by combining Lemma 3.1 and (3.3) the claim follows.  $\square$

Summing up, the idea underlying the Kernel Method consists in finding a boundary data  $g$  such that

$$(\Lambda_D - \Lambda_{bg}) g = 0, \quad (3.4)$$

and, then, to estimate the anomalous region  $D$  as the region where the electric current density vanishes, when evaluated for the reference configuration but driven by the boundary data  $g$ . The name Kernel Method comes from the key role played by the elements of the kernel of the operator  $\Lambda_D - \Lambda_{bg}$ .

Unfortunately, the Unique Continuation Principle (UCP), which has a central role for Elliptic PDEs, implies that the kernel of the operator  $\Lambda_D - \Lambda_{bg}$  is empty, as proved in the following Theorem.

**Theorem 3.3** (Weak UCP [29], [30]). *Let  $\Omega$  be a connected open subset of  $\mathbb{R}^n$ , with  $n = 2, 3$ , let  $B$  a ball contained in  $\Omega$ , and  $u \in H^1(\Omega)$  the solution of*

$$\nabla \cdot (\sigma(x) \nabla u(x)) = 0 \quad \text{in } \Omega,$$

with  $\sigma \in L_+^\infty(\Omega)$  for  $n = 2$  or  $\sigma$  Lipschitz continuous for  $n = 3$ . If  $u$  is constant in  $B$ , then  $u$  is constant in  $\Omega$ .

The UCP of Theorem 3.3 prevents to find a non-constant Dirichlet data giving a vanishing electrical field and current density in the ball  $B$ . As a consequence, the UCP combined with (3.1), gives that  $\ker\{\Lambda_D - \Lambda_{bg}\} = \{0\}$ . Indeed, if a solution  $u_{bg}$  corresponding to an element  $g$  of  $\ker\{\Lambda_D - \Lambda_{bg}\}$  is constant in a ball  $B$  contained in  $D$ , then it results to be constant over  $\Omega$ . Consequently,  $g = \sigma_{bg} \partial_n u_{bg}$  is vanishing on  $\partial\Omega$ .

This result entails a change of perspective in the imaging method. Rather than looking for a proper boundary data  $g$  such that  $\int_D \sigma_{bg}(x) |\nabla u_{bg}(x)|^2 dx = 0$ , we search for a boundary data  $g$  that is ‘‘close enough’’ to  $\ker\{\Lambda_D - \Lambda_{bg}\}$ , in the sense that it makes the difference  $\langle (\Lambda_D - \Lambda_{bg}) g, g \rangle$  small enough. Indeed, it turns out that, if the difference  $\langle (\Lambda_D - \Lambda_{bg}) g, g \rangle$  is small, then the electrical current density in the anomalous region is small accordingly.

**Lemma 3.4.** Let  $\sigma_D$  be the electrical conductivity defined in (2.3),  $\sigma_{bg}$  be the known background conductivity and  $\{g_n\}_{n \in \mathbb{N}}$  a sequence of boundary data in  $H_\diamond^{-1/2}(\partial\Omega)$ . Then

$$\lim_{n \rightarrow +\infty} \langle (\Lambda_D - \Lambda_{bg}) g_n, g_n \rangle = 0 \iff \lim_{n \rightarrow +\infty} \int_D \sigma_{bg}(x) |\nabla u_{bg}^n(x)|^2 dx = 0, \quad (3.5)$$

where  $u_{bg}$  is the solution of

$$\nabla \cdot (\sigma_{bg} \nabla u_{bg}^n(x)) = 0 \text{ in } \Omega \quad \text{and} \quad \sigma_{bg}(x) \partial_n u_{bg}^n(x) = g_n(x) \text{ on } \partial\Omega.$$

*Proof.* The claim follows by passing to the limit in (3.2).  $\square$

**Remark 3.5.** The result in Lemma 3.4 is trivial for  $g_n \rightarrow 0$ . Its usefulness is fully shown by sequences  $\{g_n\}_{n \in \mathbb{N}}$  not converging to 0.

In the next section we will show how to find such boundary data and how it can be exploited to obtain the new imaging method.

#### 4. PROPOSED METHOD

As proved in the previous section, it is not possible to find a proper boundary data  $g$  such that

$$\langle (\Lambda_D - \Lambda_{bg}) g, g \rangle = 0.$$

For this reason, we search for a boundary data  $g$  able to make arbitrary small the above quantity, i.e. the difference between the power absorbed by the actual configuration and the reference one.

In Property 1, we recall that the NtD operator is a compact operator and this ensures that  $\Lambda_D - \Lambda_{bg}$  is compact too. From the Spectral Theorem for compact operators [31], there exists a sequence  $\{g_n\}_{n \in \mathbb{N}} \subset L_\diamond^2(\partial\Omega)$  of orthonormal eigenfunctions and a sequence  $\{\lambda_n\}_{n \in \mathbb{N}}$  of corresponding positive eigenvalues such that  $\{\lambda_n\}_{n \in \mathbb{N}}$  is monotonically decreasing to zero. Let us assume the following normalization for eigenfunctions

$$\|g_n\|_2^2 = \int_{\partial\Omega} g_n^2(x) dx = 1.$$

It follows

$$\langle (\Lambda_D - \Lambda_{bg}) g_n, g_n \rangle = \langle \lambda_n g_n, g_n \rangle = \lambda_n. \quad (4.1)$$

Since the sequence  $\{\lambda_n\}_n$  is monotonically decreasing to zero, it results that a good approximation of the Kernel of  $\Lambda_D - \Lambda_{bg}$  is given by the eigenfunctions related to *sufficiently small* eigenvalues of the same operator.

Therefore, the imaging method consists in evaluating the eigenvalues and eigenvectors of  $\Lambda_D - \Lambda_{bg}$ . Then, we select the eigenfunction  $g_n$  corresponding to a small enough eigenvalue  $\lambda_n$ , as boundary data for the steady current problem (2.1) for the reference electrical conductivity  $\sigma_{bg}$ .

Since the difference  $\langle (\Lambda_D - \Lambda_{bg}) g_n, g_n \rangle = \lambda_n$  is different from zero, the ohmic power absorbed by the region  $D$  is different from zero because of Lemma 2.1 or

the UCP. Therefore, the reconstruction  $\tilde{D}$  is defined as the subset of  $\Omega$  where the power density is below a proper threshold  $\varepsilon$

$$\tilde{D} = \{x \in \Omega : \sigma_{bg}(x) |\nabla u_{bg}(x)|^2 < \|g_n\|^2 \varepsilon(\lambda_n)\}. \quad (4.2)$$

Summing up, the proposed imaging method is

- Compute experimentally or numerically  $\Lambda_{bg}$ ;
- measure the operator  $\Lambda_D$ ;
- find the eigenvalues  $\lambda_n$  and the eigenfunctions  $g_n$  of  $\Lambda_D - \Lambda_{bg}$ ;
- solve the problem (2.1) when the conductivity is  $\sigma_{bg}$  and the applied current flux at boundary  $g_n$  is an eigenfunction of  $\Lambda_D - \Lambda_{bg}$ , corresponding to a sufficiently small eigenvalue  $\lambda_n$ ;
- the reconstructed anomaly is given by (4.2).

The threshold  $\varepsilon$  is chosen coherently with the value of  $\lambda_n$ , while the value of  $n$  is chosen according to the noise level. Details about the selection of the threshold  $\varepsilon$  and the index  $n$  are given in the next section.

## 5. TREATMENT OF THE NOISE

In any practical application, only a noisy version of the DtN map is available. Specifically, it is supposed that the noisy measurements can be modeled as

$$\Delta\tilde{\Lambda} = \Delta\Lambda + N, \quad (5.1)$$

where  $\Delta\tilde{\Lambda}$  is the noisy version of the noise free difference operator  $\Delta\Lambda = \Lambda_D - \Lambda_{bg}$ , and  $N$  is the operator representing the noise.

Hereafter it is assumed that  $N$  is a bounded operator, i.e.  $\|N\| < +\infty$ , where:

$$\|N\| = \sup_{f \in L^2(\partial\Omega)} \frac{\|Nf\|_2}{\|f\|_2}$$

Moreover, the operator  $N$  can always be considered self-adjoint, by taking the symmetric part of  $\Delta\tilde{\Lambda}$ . Under these assumptions, the spectrum of  $\Delta\tilde{\Lambda}$  can be related to the one of  $\Delta\Lambda$  via the following proposition, which is an application of standard arguments in perturbation theory [32]

**Proposition 5.1.** *Let  $\Delta\tilde{\Lambda}$  as defined in (5.1), where  $N$  is a bounded and self-adjoint operator, and  $\delta = \|N\|$ . Let  $\lambda_k, \tilde{\lambda}_k$  be the eigenvalues of  $\Lambda_D - \Lambda_{bg}$  and  $\Delta\tilde{\Lambda}$ , respectively, ordered in a decreasing order. Then*

$$|\tilde{\lambda}_k - \lambda_k| \leq \delta$$

Proposition 5.1 allows to quantitatively evaluate the impact of the noise on the eigenvalues of the key operator  $\Lambda_D - \Lambda_{bg}$ . Specifically, given the noise level  $\delta$  as the norm of the noise operator  $N$ , the eigenvalues of  $\Delta\tilde{\Lambda}$  differ at most of  $\delta$  from the corresponding eigenvalues of the noise free operator  $\Lambda_D - \Lambda_{bg}$ . Therefore, all the eigenvalue/eigenfunction pairs with eigenvalue smaller than  $\delta$  are not reliable, since

corrupted by the noise. An example is shown in Figure 1, where the eigenvalues

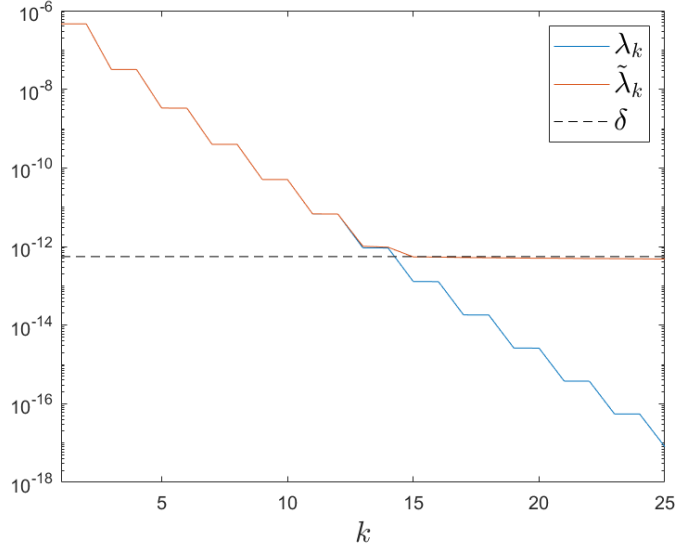


FIGURE 1. Perturbation of the eigenvalues of the key operator  $\Delta\Lambda$ . The domain  $\Omega$  is a circle centered in the origin with radius 10 cm, while the anomaly  $D$  is a circle centered in the origin and radius 4 cm. The electrical conductivities are  $\sigma_{bg} = 200$  S m and  $\sigma_a = 1$  S m. The norm of the operator  $N$  is  $\delta$ .

of the perturbed operator are plateauing when their amplitude is of the order of  $\delta$ . It is remarkable how they differ from that of the noise free operator  $\Delta\Lambda$ .

As highlighted in Section 4, the eigenfunction  $g_n$  is chosen to get  $\langle \Delta\Lambda g_n, g_n \rangle = \lambda_n \|g_n\|^2$  as close as possible to zero, in order to mimic an element of (void) the kernel of the operator  $\Lambda_D - \Lambda_{bg}$ . In the presence of noisy data, this translates in the eigenfunction  $\tilde{g}_n$  corresponding to the smallest eigenvalue  $\tilde{\lambda}_n$  above the noise level  $\delta$ . The latter can be easily identified because of the presence of the plateau appearing at about  $\delta$ .

The remaining part of this section is devoted to the choice of the threshold  $\varepsilon$  appearing in the reconstruction rule of (4.2). This threshold plays a key role.

Preliminary, the following proposition is proven, which establish the relationship between the measured data, i.e.  $\Delta\tilde{\Lambda}$ , and the ohmic power absorbed by the unknown anomalous region.

**Proposition 5.2.** *Let  $\Delta\tilde{\Lambda}$  be the noisy data defined in (5.1), where  $\Delta\Lambda = \Lambda_D - \Lambda_{bg}$  is the noise free operator and  $N$  is a bounded noise operator with  $\|N\| \leq \delta$ .*

Let  $u_{bg}$  the solution of problem (2.1) for an electrical conductivity  $\sigma(x) = \sigma_{bg}(x)$  and an applied boundary data  $g$ , then

$$\frac{\sigma_a^m}{\Delta\sigma} \left( \langle \Delta\tilde{\Lambda} g, g \rangle - \delta \|g\|^2 \right) \leq \int_D \sigma_{bg}(x) |\nabla u_{bg}(x)|^2 dx \leq \frac{\sigma_{bg}^M}{\Delta\sigma} \left( \langle \Delta\tilde{\Lambda} g, g \rangle + \delta \|g\|^2 \right), \quad (5.2)$$

where  $D$  is the unknown anomalous region and  $\Delta\sigma_G = \sigma_{bg}^m - \sigma_a^M$ .

*Proof.* From Equation (3.2) (see proof of Lemma 3.1), it follows

$$\frac{\sigma_a^m}{\Delta\sigma_G} \langle \Delta\Lambda g, g \rangle \leq \int_D \sigma_{bg} |\nabla u_{bg}|^2 dx \leq \frac{\sigma_{bg}^M}{\Delta\sigma_G} \langle \Delta\Lambda g, g \rangle. \quad (5.3)$$

The noise free data can be related to the measured ones due to the (5.1), leading to  $\langle \Delta\Lambda g, g \rangle = \langle \Delta\tilde{\Lambda} g, g \rangle - \langle N g, g \rangle$ . Moreover, recalling the definition of operator norm [32, Ch.1 Par. 4.1]

$$-\delta \|g\|^2 \leq \langle N g, g \rangle \leq \delta \|g\|^2,$$

hence,

$$\langle \Delta\tilde{\Lambda} g, g \rangle - \delta \|g\|^2 \leq \langle \Delta\Lambda g, g \rangle \leq \langle \Delta\tilde{\Lambda} g, g \rangle + \delta \|g\|^2. \quad (5.4)$$

By combining (5.3) and (5.4), the claim follows.  $\square$

Proposition 5.2 gives an estimation for the ohmic power absorbed by the anomaly based only on available quantities: the measured data  $\Delta\tilde{\Lambda}$ , the noise level  $\delta$  and the upper and lower bounds  $\sigma_a^m$ ,  $\sigma_a^M$ ,  $\sigma_{bg}^m$  and  $\sigma_{bg}^M$  to the electrical conductivities. Proposition 5.2 set a constraint, in the sense that a proper reconstruction method has to provide a reconstruction of the anomalous region  $D$  satisfying (5.2).

In the Kernel Method the anomalous region is evaluated by applying to the reference configuration a proper eigenfunction  $g_n$  of the difference operator  $\Delta\Lambda$ . In the presence of noise, only the eigenfunctions  $\tilde{g}_n$  of the noisy operator  $\Delta\tilde{\Lambda}$  can be computed. By specializing Proposition 5.2 for  $g = \tilde{g}_n$ , it holds

$$\frac{\sigma_a^m}{\Delta\sigma_G} \left( \tilde{\lambda}_n - \delta \right) \|\tilde{g}_n\|^2 \leq \int_D \sigma_{bg}(x) |\nabla u_{bg}(x)|^2 dx \leq \frac{\sigma_{bg}^M}{\Delta\sigma_G} \left( \tilde{\lambda}_n + \delta \right) \|\tilde{g}_n\|^2. \quad (5.5)$$

The above equation suggests to define a threshold on the ohmic power absorbed by the anomaly, instead of directly on the power density. Specifically, let  $D_\alpha$  be defined as

$$D_\alpha = \{x \in \Omega \mid \sigma_{bg}(x) |\nabla u_{bg}(x)|^2 < \alpha\},$$

then the reconstructed region is  $D_{\alpha^*}$ , where  $\alpha^*$  is the unique solution of

$$\int_{D_\alpha} \sigma_{bg} |\nabla u_{bg}|^2 dx = \varepsilon^* \|\tilde{g}_n\|^2, \quad (5.6)$$

with respect to  $\alpha$ . In (5.6) the parameter  $\varepsilon^*$  satisfies

$$\frac{\sigma_a^m}{\Delta\sigma_G} \left( \tilde{\lambda}_n - \delta \right) \leq \varepsilon^* \leq \frac{\sigma_{bg}^M}{\Delta\sigma_G} \left( \tilde{\lambda}_n + \delta \right), \quad (5.7)$$

Summing up, the Kernel Method for noisy data is

- Measure experimentally or compute numerically  $\Lambda_{bg}$ ;
- measure the noisy data  $\tilde{\Lambda}_{\sigma_D}$ ;
- compute numerically the eigenvalues  $\{\tilde{\lambda}_k\}_k$  and the eigenfunctions  $\{\tilde{g}_k\}_k$  of  $\Delta\tilde{\Lambda}$ ;
- identify the last significant eigenvalue  $\tilde{\lambda}_{k^*}$  of  $\Delta\tilde{\Lambda}$  above the plateau and the corresponding eigenfunction  $\tilde{g}_{k^*}$ ;
- solve the problem (2.1) when the conductivity is  $\sigma_{bg}$  and the applied boundary data is  $\tilde{g}_{k^*}$ ;
- find the value of  $\alpha^*$  that solves (5.6). The reconstruction of the unknown anomaly is, therefore,  $D_{\alpha^*}$ .

## 6. ANALYTICAL EXAMPLES

In this Section, some examples on canonical geometries are presented to clarify the main features of the proposed method and its limits.

The reference geometry presents radial symmetry and, therefore, the eigenvalues and eigenfunctions of  $\Lambda_D - \Lambda_{bg}$  can be evaluated analytically.

The data are assumed to be noise free, i.e.  $\delta = 0$ . In this case, there are two main customizations of the method presented in Section 5, following condition  $\delta = 0$ : (i) the plateau is at the value 0, and (ii) the compatibility condition of (5.7) reduces to

$$\frac{\sigma_a^m}{\Delta\sigma_G} \lambda_n \leq \varepsilon^* \leq \frac{\sigma_{bg}^M}{\Delta\sigma_G} \lambda_n. \quad (6.1)$$

The first case (see Section 6.1) refers to a circular anomaly in a circular domain. This case exemplify for a 2D case the main steps of the method. The second case (see Section 6.2) highlights a limit of the method consisting in its inability in retrieving anomaly with holes.

**6.1. Concentric circles.** The first configuration consists in an unknown circular anomaly  $D$  embedded in a circular domain  $\Omega$ , as shown in Figure 2. The anomaly  $D$  has radius  $r_i$ , while the domain  $\Omega$  has radius  $R$ . The anomaly  $D$  consists of a homogeneous disk of electrical conductivity  $\sigma_a$ , while the background consists of a homogeneous material of electrical conductivity  $\sigma_{bg}$ .

In this configuration, the eigenfunctions  $g_n$  of  $\Lambda_D - \Lambda_{bg}$  are given by  $g_n(\theta) = \frac{1}{\sqrt{\pi}} \cos(n\theta)$ ,  $\forall n \in \mathbb{N}$ , while the corresponding eigenvalues are

$$\lambda_n = \frac{R}{\sigma_{bg} |n|} \frac{2 \left(\frac{r_i}{R}\right)^{|n|} (\sigma_{bg} - \sigma_a)}{\left(\frac{r_i}{R}\right)^{|n|} (\sigma_a - \sigma_{bg}) + \left(\frac{R}{r_i}\right)^{|n|} (\sigma_a + \sigma_{bg})}.$$

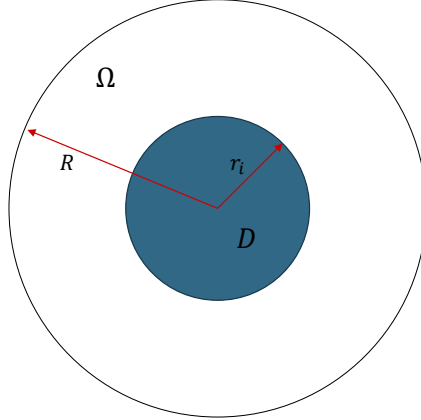


FIGURE 2. The Kernel Method is applied to retrieve the unknown anomaly  $D$ .

For a given eigenfunction  $g_n$  applied as Neumann boundary data to the reference configuration ( $\sigma(x) = \sigma_{bg}$  in  $\Omega$ ), the corresponding solution  $u_{bg}^n$  of (2.1) is

$$u_{bg}^n(r, \theta) = \frac{R}{n\sqrt{\pi}\sigma_{bg}} \left(\frac{r}{R}\right)^n \cos(n\theta),$$

with a related power density given by

$$p_n(r, \theta) = \sigma_{bg} |\nabla u_{bg}|^2 = \frac{1}{\sigma_{bg}\pi} \left(\frac{r}{R}\right)^{2n-2}. \quad (6.2)$$

As already pointed out in Section 5, the unknown anomaly is reconstructed by solving the equation

$$\int_{D_\alpha} \sigma_{bg} |\nabla u_{bg}|^2 dx = \varepsilon^* \|g_n\|^2, \quad (6.3)$$

with respect to  $\alpha$ , where  $D_\alpha$ , in this specific case, is given by

$$D_\alpha = \left\{ x \in \mathbb{R}^2 \mid \frac{1}{\sigma_{bg}\pi} \left(\frac{r}{R}\right)^{2n-2} < \alpha \right\}$$

and  $\varepsilon^*$  fulfills the following constraint

$$\frac{\sigma_a}{\sigma_{bg} - \sigma_a} \lambda_n \leq \varepsilon^* \leq \frac{\sigma_{bg}}{\sigma_{bg} - \sigma_a} \lambda_n,$$

which is derived from (6.1) for homogeneous conductivities. Supposing  $\sigma_{bg} > 2\sigma_a$ , a possible choice is given by  $\varepsilon^* = \lambda_n$ .

Recognizing that, for every  $\alpha > 0$ , the set  $D_\alpha$  is a circle centered in the origin and that  $\|g_n\| = 1$ , equation (6.3) becomes

$$\int_0^{2\pi} \int_0^{\tilde{r}_i} \frac{1}{\sigma_{bg}\pi} \left(\frac{r}{R}\right)^{2n-2} dr d\theta = \lambda_n$$

which gives

$$\tilde{r}_i(n) = R \left( \frac{n\sigma_{bg}}{R^2} \lambda_n \right)^{\frac{1}{2n}}. \quad (6.4)$$

In Figure 3, the behavior of  $\tilde{r}_i$  with respect to the order of the chosen eigenfunction

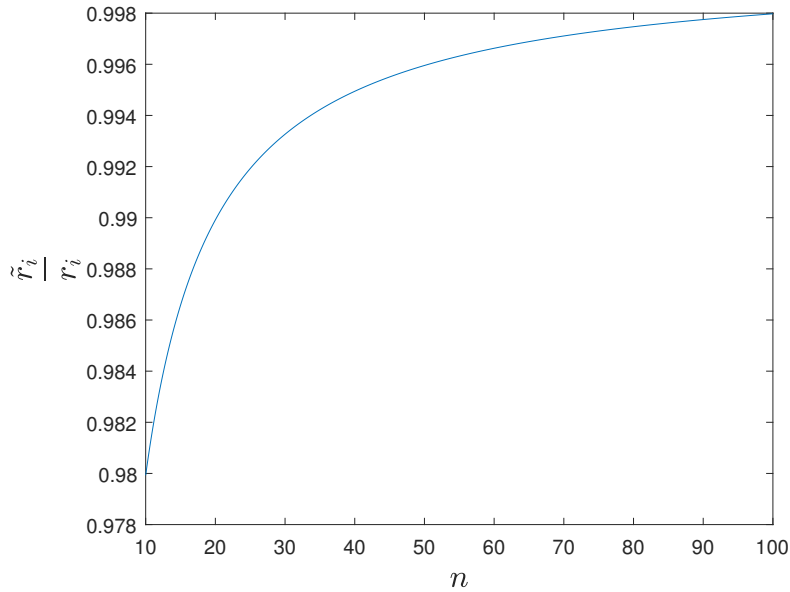


FIGURE 3. Behavior of the reconstructed internal radius  $\tilde{r}_i$ , with respect to the order of the selected eigenfunction.

is depicted. As it can be seen, the reconstructed radius tends to the actual one for  $n \rightarrow +\infty$ .

**6.2. Holed circle.** This example aims to clearly show one of the limits of the proposed method, which is related to the underlying physical model of the problem. Consider the configuration depicted in Figure 4, where the aim is to retrieve the anomalous region occupying the circular crown  $r_1 \leq r \leq r_2$ . The external radius of the circle is  $r_3$  and the electrical conductivities are homogeneous and equal to  $\sigma_a$  in the circular crown and  $\sigma_{bg}$  elsewhere. A standard application of the separation

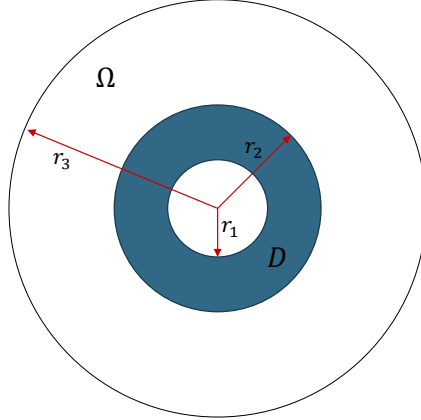


FIGURE 4. The Kernel Method is applied to retrieve the circular crown  $r_1 \leq r \leq r_2$ .

of variables leads to

$$g_n(\theta) = \frac{1}{\sqrt{\pi}} \cos(n\theta)$$

$$\lambda_n = \frac{r_3}{n\sigma_{bg}} \frac{2 \left(\frac{r_2}{r_3}\right)^n \left[\left(\frac{r_1}{r_2}\right)^n - \left(\frac{r_2}{r_1}\right)^n\right] (\sigma_{bg}^2 - \sigma_d^2)}{d_n}$$

$$d_n = \left(\frac{r_1}{r_2}\right)^n \left[ \left(\frac{r_3}{r_2}\right)^n (\sigma_d - \sigma_{bg})^2 + \left(\frac{r_2}{r_3}\right)^n (\sigma_d^2 - \sigma_{bg}^2) \right]$$

$$- \left(\frac{r_2}{r_1}\right)^n \left[ \left(\frac{r_3}{r_2}\right)^n (\sigma_d + \sigma_{bg})^2 + \left(\frac{r_2}{r_3}\right)^n (\sigma_d^2 - \sigma_{bg}^2) \right].$$

As for the previous example, the Kernel Method requires one to drive the reference configuration with one of the eigenfunctions  $g_n$  and, then, to evaluate the power density on the same configuration. The expression for the power density is that of (6.2), when replacing  $R$  with  $r_3$ .

Equation (6.2) suggests that it is not possible to reconstruct the circular crown, due to the fact that the power density is a monotonic function of the radial coordinate  $r$ . This reflects a physical limit. Indeed, the Kernel Method attempts to find a proper boundary data able to generate a current density flowing outside the anomalous region. It is evident that there is no pathway for the current density to circulate in the inner region  $r < r_1$ , without crossing the circular crown.

However, the method is still able to correctly retrieve the outer boundary of the circular crown, as can be seen in Figure 5. The reconstructed radius is obtained from

$$\tilde{r}_2(n) = R \left( \frac{n\sigma_{bg}}{r_3^2} \lambda_n \right)^{\frac{1}{2n}}, \quad (6.5)$$

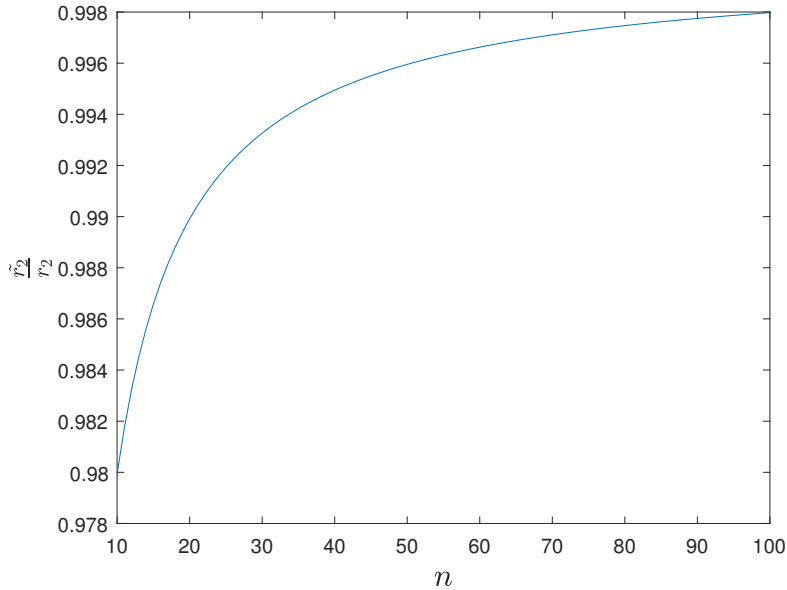


FIGURE 5. Behavior of the reconstructed outer radius  $\tilde{r}_2$  of the circular crown, with respect to the order of the selected eigenfunction.

which tends to  $r_2$  as  $n \rightarrow \infty$ .

## 7. NUMERICAL EXAMPLES

This last section is dedicated to showing the effectiveness of the proposed method in some examples of application. Specifically, the aim is to determine the shape, position and dimension of one or more anomalies less conductive than the background material. This is a typical case in applications where the ERT is employed to determine defects in conductive materials.

The data are simulated by an in-house FEM code, based on the Galerkin method. The domain  $\Omega$  is a circle with radius  $r = 2.5$  cm and it is discretized in 16 384 triangular elements, while the boundary  $\partial\Omega$  is given by  $N_b = 256$  elements of the same length. The mesh has  $N_p = 8321$  nodes. The electric potential is discretized with a piece-wise linear function, as the boundary potential, while the imposed normal component of current density  $g$  is discretized by a piece-wise constant function on the boundary elements. In this discrete setting, the NtD operator is a linear map from  $\mathbb{R}^{N_b-1}$  to  $\mathbb{R}^{N_b-1}$ , taking into account the constraint of vanishing integral mean on the boundary for both the applied current density and the measured voltages.

All the reconstructions are obtained by adding synthetic noise on the data. Specifically, the following noise model is adopted, which is the discrete counterpart

of (5.1)

$$\begin{aligned}\Delta\tilde{\mathbf{R}} &= \mathbf{R}_D - \mathbf{R}_{bg} + \eta\delta_R\mathbf{N} \\ \delta_R &= \max_{i,j} |R_D(i,j) - R_{bg}(i,j)| \\ \mathbf{N} &= \frac{\mathbf{A} + \mathbf{A}^T}{2} \\ A(i,j) &\sim \mathcal{N}(0,1)\end{aligned}$$

where  $\mathbf{R}_D$  and  $\mathbf{R}_{bg}$  are the discretization of  $\Lambda_D$  and  $\Lambda_{bg}$  on a finite subspace of  $L^2_\diamond(\partial\Omega)$ , respectively,  $\Delta\tilde{\mathbf{R}}$  is the noisy version of  $\mathbf{R}_D - \mathbf{R}_{bg}$  and  $\eta$  is a constant controlling the noise level.

The background material has a uniform electrical conductivity equal to  $\sigma_{bg} = 200$  S/m while the electrical conductivity of the anomaly  $D$  is equal to  $\sigma_a = 1$  S/m.

The threshold  $\varepsilon^*$  (see equation 5.6) is set to  $\tilde{\lambda}_n$ , which is a feasible choice since  $\sigma_{bg} > 2\sigma_a$  (see also Section 6.1).

The reconstructions are reported in Figures 6 and 7, where a suitable set of different configurations is proposed to test various aspects of the imaging method. From these Figures, it is possible to infer that, at a realistic noise level, the reconstructions are of high quality. Specifically, we highlight (i) excellent performances on convex anomalies (A, B, D, F, G, J), (ii) possibility of resolving multiple anomalies (H, N, O), (iii) tendency to convexification (C, E, I, K, L, M), and (iv) impossibility of reconstructing the interior of an anomaly with cavities (I).

## 8. CONCLUSIONS

In this work, a new non-iterative imaging method for Electrical Resistance Tomography is presented. Specifically, the method is meant for the inverse obstacle problem, where the aim is to retrieve an unknown anomaly embedded in a known background. The method relies on the possibility to find a boundary data  $g$  producing a current density that is mostly vanishing in the regions occupied by the anomaly, when  $g$  is applied to the reference configuration without anomaly.

The imaging method, characterized by a very simple and stable numerical implementation, provides a simple way to evaluate this special boundary data  $g$ .

The numerical examples demonstrate that the proposed algorithm achieves excellent performances in the presence of noise, also.

## 9. ACKNOWLEDGMENT

This work was supported by the Italian Ministry of University and Research under the PRIN-2022, Grant Number 2022Y53F3X “Inverse Design of High-Performance Large-Scale Metalenses ”.

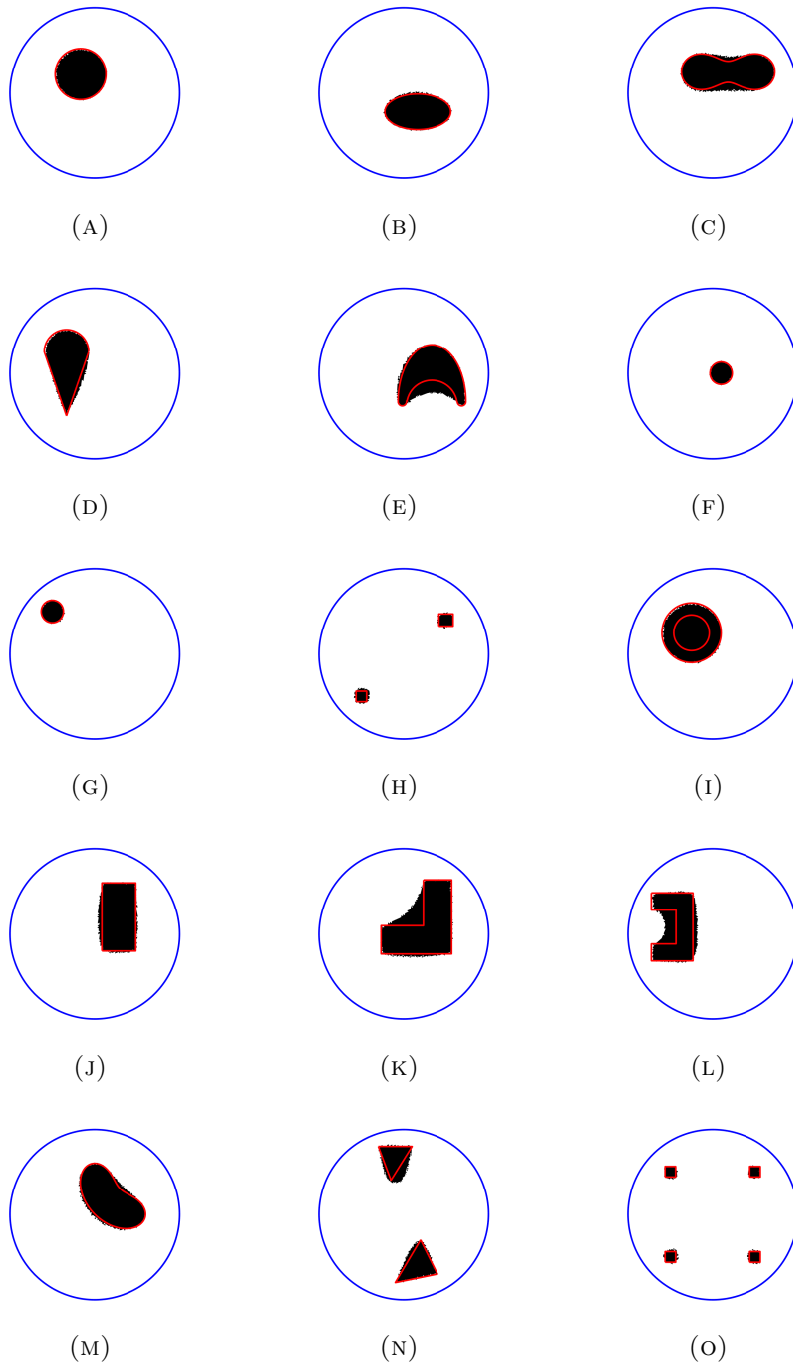


FIGURE 6. Reconstructions for  $\eta = 0$  (within the machine precision). In black the reconstructed anomaly  $\tilde{D}$ , while in red the boundary of the actual anomaly  $D$ .

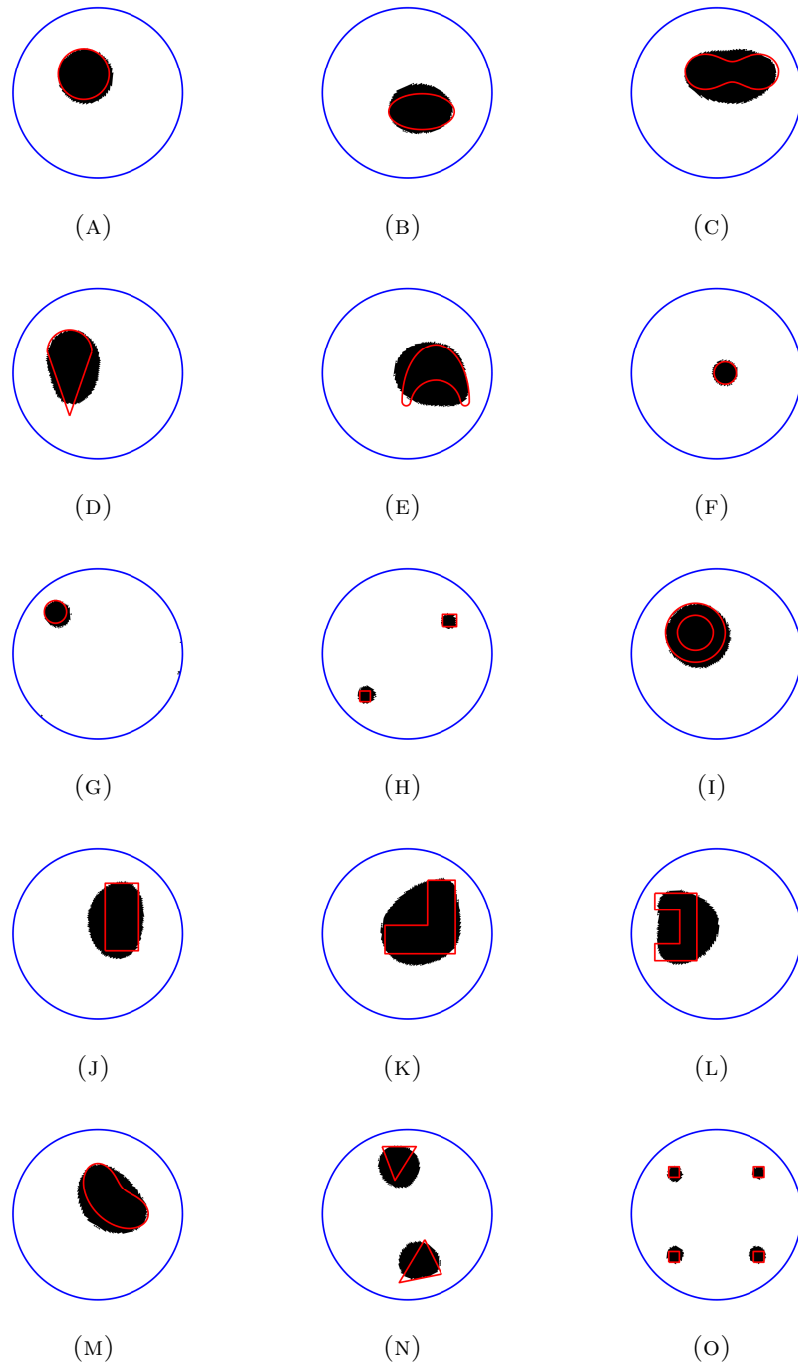


FIGURE 7. Reconstructions for  $\eta = 10^{-3}$ . In black the reconstructed anomaly  $\tilde{D}$ , while in red the boundary of the actual anomaly  $D$ .

## AUTHORSHIP CONTRIBUTION STATEMENT

**A. Tamburrino:** Conceptualization, Methodology, Formal analysis, Writing, Supervision.

**V. Mottola:** Conceptualization, Methodology, Formal analysis, Writing.

## REFERENCES

- [1] Cheng J, Liu S and Li Y 2019 Design and optimization of liquid level sensor based on electrical tomography *2019 IEEE International Conference on Imaging Systems and Techniques (IST)* pp 1–6
- [2] Durdevic P, Hansen L, Mai C, Pedersen S and Yang Z 2015 *IFAC-PapersOnLine* **48** 147–153 ISSN 2405-8963 2nd IFAC Workshop on Automatic Control in Offshore Oil and Gas Production OOGP 2015
- [3] Mann R 2009 Ert imaging and linkage to cfd for stirred vessels in the chemical process industry *2009 IEEE International Workshop on Imaging Systems and Techniques* pp 218–222
- [4] Holder D 1994 *Thorax* **49** 626–626
- [5] Tarassenko L and Rolfe P 1984 *Electron. Lett.* **20** 574
- [6] Meier T, Luepschen H, Karsten J, Leibecke T, Grossherr M, Gehring H and Leonhardt S 2008 *Intensive Care Med.* **34** 543–550
- [7] Adler A, Berthiaume Y, Guardo R and Amyot R 1995 *Proceedings of 17th International Conference of the Engineering in Medicine and Biology Society* **1** 557–558 vol.1 URL <https://api.semanticscholar.org/CorpusID:61366527>
- [8] Conway J 1987 *Clin. Phys. Physiol. Meas.* **8** 141–146
- [9] Pham T M T, Yuill M, Dakin C and Schibler A 2011 *Eur. Respir. J.* **37** 919–924
- [10] Zain N M and Chelliah K K 2014 *Asian Pac. J. Cancer Prev.* **15** 1327–1331
- [11] Holder D S, Rao A and Hanquan Y 1996 *Physiol. Meas.* **17** A179–A186
- [12] Kruger M V P 2003 Tomography as a metrology technique for semiconductor manufacturing Tech. Rep. UCB/ERL M03/11 EECS Department, University of California, Berkeley
- [13] Jordana J, Gasulla M and Pallàs-Areny R 2001 *Measurement Science and Technology* **12** 1061–1068
- [14] Hou T C, Loh K J and Lynch J P 2007 *Nanotechnology* **18** 315501
- [15] Linderholm P, Marescot L, Loke M H and Renaud P 2008 *IEEE Transactions on Biomedical Engineering* **55** 138–146
- [16] Lionheart W R B 2004 *Physiological Measurement* **25** 125 URL <https://dx.doi.org/10.1088/0967-3334/25/1/021>
- [17] Colton D and Kirsch A 1996 *Inverse Problems* **12** 383 URL <https://dx.doi.org/10.1088/0266-5611/12/4/003>
- [18] Kirsch A 1998 *Inverse Problems* **14** 1489
- [19] Brühl M 2001 *SIAM Journal on Mathematical Analysis* **32** 1327–1341
- [20] Ikehata M 1999 *Journal of Inverse and Ill-posed Problems* **7** 255–272 URL <https://doi.org/10.1515/jiip.1999.7.3.255>
- [21] Devaney A J Super-resolution processing of multi-static data using time reversal and music northeastern University preprint
- [22] Tamburrino A and Rubinacci G 2002 *Inverse Problems* **18** 1809–1829
- [23] Mottola V, Esposito A C, Faella L, Piscitelli G, Prakash R and Tamburrino A 2025 The inverse obstacle problem for nonlinear inclusions (*Preprint* 2408.08040) URL <https://arxiv.org/abs/2408.08040>
- [24] Gisser D G, Isaacson D and Newell J C 1990 *SIAM Journal on Applied Mathematics* **50** 1623–1634
- [25] Gebauer B 2008 *Inverse Problems & Imaging* **2** 251–269
- [26] Harrach B and Ullrich M 2013 *SIAM Journal on Mathematical Analysis* **45** 3382–3403
- [27] Ikehata M 1998 *Journal of Inverse and Ill-Posed Problems* **6** 127–140

- [28] Calderon A P 1980 On an inverse boundary *Seminar on Numerical Analysis and its Applications to Continuum Physics, Rio de Janeiro, 1980* (Brazilian Math. Soc.) pp 65–73
- [29] Alessandrini G 2012 *Journal of Mathematical Analysis and Applications* **386** 669–676 ISSN 0022-247X
- [30] Garofalo N and Lin F 1986 *Indiana University Mathematics Journal* **35** 245–268
- [31] Rudin W 1991 *Functional Analysis* 2nd ed International series in pure and applied mathematics (McGraw-Hill) ISBN 0070542368; 9780070542365
- [32] Kato T 1995 *Perturbation theory for linear operators* Classics in Mathematics (Springer) ISBN 9783540586616,354058661X